FE-2516-7
Distribution Category UC-90e

CENTRIFUGAL FLUIDIZED COMBUSTION OF COAL

Quarterly Report for the
Period April - June 1978

Edward K. Levy
John C. Chen

LEHIGH UNIVERSITY
Bethlehem, Pennsylvania 18015

Date written - July 1978

PREPARED FOR THE UNITED STATES
DEPARTMENT OF ENERGY
Under Contract No. E(49-18)-2516

CENTRIFUGAL FLUIDIZED COMBUSTION OF COAL

by

Edward K. Levy
John C. Chen

ABSTRACT

Experiments were performed with styrene bed material to determine the influence of bed density and particle size distribution on CFB fluidization characteristics. Comparisons between the styrene data, previous data using glass bed material, and the theoretical equations for bed pressure drop and minimum fluidization show excellent agreement between theory and experiment for all cases. Laboratory preparations are underway for experiments on particle elutriation from a CFB. In addition, preliminary data were obtained on the velocity profiles in the freeboard region of a CFB. Sample profiles are presented for one set of operating conditions.

An analysis of the energy costs for a CFB coal combustor operating in a combined cycle is described. When compared to energy costs for other fossil-fired power generation systems, the results indicate the CFB system has excellent potential, particularly for peak power generation applications.

OBJECTIVE AND SCOPE OF WORK

Conventional fluidized bed combustors, with the bed material fluidized against the force of gravity, have many desirable features. However, for large capacity power generation applications or with very fine bed material, these systems require extremely large distributor areas, causing difficulties with start-up, solids feed, bed mixing, and turndown. The centrifugal fluidized bed (Figure 1) rotates about its axis of symmetry and the fluidizing air flows radially inward through the porous cylindrical surface of the distributor. The inward drag force of the fluidizing air on the bed material is balanced by the large radial accelerations caused by the rotational motion, permitting much larger air flow rates per unit volume than are possible with a conventional fluidized bed operating against gravity. By varying the speed of rotation of the bed, the flow rate of air, and the bed temperature, it should be possible to achieve considerable variation in system power output providing the capability for operating over a wide range of part-load conditions. In addition, the added flexibility due to bed rotation and the small size of the system should ease the problem of start-up. With a bed material of dolomite or limestone to capture SO_2, the centrifugal combustor could be used to burn high sulfur coal and coal char.

The centrifugal combustor would be operated as an adiabatic device with sufficient excess air to maintain bed temperatures in the desired range. For power generation applications, it might be used as the combustor in a combined gas turbine/steam turbine cycle (Figure 2).

The successful development of the centrifugal fluidized bed concept would provide a system for coal or char combustion which would be compact, clean, efficient, and which would have the capabilities of being operated at full or part-load conditions. The system might be used for utility size plants or for smaller industrial power generation applications.

The objective of the program is to determine the feasibility of operating a centrifugal fluidized bed in a continuous mode. Task I consists of a series of experiments using a model of a fluidized bed combustor operated at room temperature and pressure. Fluidized bed materials which simulate coal and/or coal char in specific gravity, particle size and distribution will be used to determine the requirements for minimum fluidization, bed pressure drop, freeboard pressure drop, and the extent of particle elutriation. The constraints affecting the addition and removal of material from the bed will be determined.

The second task involves experiments to study the fluid mechanics of confined vortex flows without particles. Previous work on confined vortex flows indicates nonuniformities in radial velocity, secondary flow patterns, and flow instabilities can occur in a single phase vortex gas flow. If these persist in the bed region of a centrifugal fluidized bed, they could affect bed stability, minimum fluidization and particle elutriation. This work is intended to develop criteria

for the flow regimes in which significant secondary flow patterns occur. Once the proper criteria are established, comparisons will be made with the experiments on rotating fluidized beds to determine if the nonuniformities affect the bed stability and the quality and uniformity of fluidization.

SUMMARY OF PROGRESS TO DATE

Laboratory test units for batch experiments on bed stability, minimum fluidization, and start-up were built; and experiments on bed start-up and minimum fluidization were performed. Analyses for bed pressure drop, minimum fluidization, and bed shape were developed, the results of which were compared to experimental data on the influence of operating parameters such as particle density, particle diameter, particle size distribution, angular velocity, bed thickness, and grid taper angle on fluidization. Two test sections for experiments on feeding and removal of solids were designed, fabricated, installed and calibrated, and experiments on solids feeding and removal were performed.

One of the batch test sections was modified, adapting the unit for measurement of tangential and radial velocity profiles within the rotating chamber. A fiber x-probe was calibrated for three-dimensional measurements of air velocity within the test section. A probe traversing mechanism was designed and fabricated and experiments to gather data on the influence of flow rate and rotation in the confined vortex flow on flow regime were initiated.

A project schedule is given in Figure 3.

DETAILED DESCRIPTION OF TECHNICAL PROGRESS

TASK 1

- Batch Experiments on Minimum Fluidization and Bed Pressure Drop

During the first year of the contract, detailed experiments were performed to determine the effects of distributor design, bed angular velocity, and bed mass on minimum fluidization and bed pressure drop. The data show that the relationship between bed pressure drop and air flow rate is similar qualitatively to that of a conventional fluidized bed, with generally good agreement between the experimental results and theoretical predictions.

Two parameters which were not studied in the earlier experiments are the density and size distribution of the bed material. All of the previous experiments were performed with glass beads (2.47 grams per cc) with a relatively narrow size distribution. The theoretical equations

for bed pressure drop and minimum fluidization do show effects of these parameters. If the bed is packed locally, the bed pressure drop is given by the relation

$$\Delta P_{BED} = \frac{150(1-\varepsilon)^2}{\varepsilon^3(d_p)^2} \mu u_o r_o \ell n(r_o/r_i) + \frac{1.75(1-\varepsilon)}{\varepsilon^3 d_p} \rho_f (r_o u_o)^2 \left[\frac{1}{r_i} - \frac{1}{r_o}\right] \quad (1)$$

where $\bar{d}_p$ is the mean diameter of the bed material and is equal to

$$\bar{d}_p = \sum \frac{1}{\frac{x_i}{d_{p_i}}} \quad (2)$$

If the bed is fluidized, the bed pressure drop equals

$$\Delta P_{BED} = (\rho_s - \rho_f)(1-\varepsilon)\omega_o^2 \frac{[r_o^2 - r_i^2]}{2} \quad (3)$$

where ρ_s is the density of the bed material. The radial velocity at minimum fluidization, calculated at the outer radius of the bed, equals

$$Ga = \frac{300(1-\varepsilon)\ell n(r_o/r_i)}{\varepsilon^3 \phi^2 [1 - (\frac{r_i}{r_o})^2]} Re + \frac{3.50[\frac{r_o}{r_i} - 1]}{\varepsilon^3 \phi [1 - (\frac{r_i}{r_o})^2]} Re^2 \quad (4)$$

During the last quarter, additional experiments were performed to study the effects of density and particle size distribution. These experiments were performed in the same apparatus used for the earlier batch tasks. This unit consists of a 12 inch diameter by 6 inch high distributor contained in a stationary air plenum. The distributor is tapered and its surface is fabricated from reinforced fine mesh screen. The system can be operated with air flow rates to 1200 scfm and with distributor angular velocities above 350 rpm. The bed material was styrene divinyl benzene beads supplied by the Dow Chemical Company. This material is spherical in shape with a specific gravity of 1.05 grams per cc.

The first series of tests was performed with styrene beads with a narrow size distribution centered around 775 μm. Shown in Figure 4 is a plot of bed pressure drop versus air flow rate with 0.68 kg of bed material at angular velocities of 200, 300 and 400 rpm. At minimum fluidization this corresponds to an average bed thickness of approximately 0.35 inches. The solid curves are the theoretical results predicted by the analysis described in Reference 1. The effects of the bed mass (bed thickness) on fluidization are shown in Figure 5. In this case all of the experiments were performed at an angular velocity of 300 rpm. Here minimum fluidization is a relatively weak function of bed thickness; however, the bed pressure drop depends strongly on the amount of bed material. Figures 6 and 7 give a direct comparison between the glass and plastic bed materials, illustrating the influence of bed density on fluidized bed pressure drop and minimum fluidization. Although the experiments were not performed with the same average particle diameters for the plastic and glass samples, the excellent agreement between theory and experiment for both densities is an indication of the validity of the model.

After completing the tests with a narrow size distribution of bed material, a second series of experiments was performed with a relatively wide size distribution. Once again, the styrene bed material was used, but with the size distribution shown in Figure 8. The mean particle diameter for the sample is 713 μm. Shown in Figures 9 and 10 are comparisons between the pressure drop-flow rate curves for the two cases. The pressure drop in the packed bed region seems to be predicted very well by equation (1) using the mean particle diameter given by equation (2). The primary difference between the two cases appears in the transition between packed and fluidized states, where the wider distribution exhibits a wider transition range.

According to equation (4), minimum fluidization velocity depends on the inner and outer radii of the bed r_i and r_o. This functional dependence is illustrated in Figure 11, where the theoretical Reynolds number at minimum fluidization, Re_{mf}, is plotted versus Galileo number for several values of r_o/r_i. The experimental data are in generally good agreement with the theory.

One of the potential advantages of the centrifugal fluidized bed combustor over the conventional one "g" system is the ability to achieve a wide turndown range. Whereas the output of a conventional fluidized bed combustor is varied primarily by changing the velocity of the fluidizing gas, the output of the CFB combustor can be varied over a much wider range by changing both the speed of rotation and the velocity of the fluidizing gas. This feature is illustrated in Figure 12 where the solid curves are the theoretical pressure drop-flow rate characteristics of the bed for five different values of speed of rotation. The symbols and dashed curve show the data obtained in an experiment in which the bed was first operated at 450 rpm and 0.42 scms. The air flow rate was then decreased to nearly minimum fluidization conditions. Additional turndown was achieved by simultaneously

reducing the rpm and air flow rate to a final state of 200 rpm at 0.13 scms. The turndown range in this experiment (approximately 3/1) was limited by the capacity of the compressed air system and could have been extended by starting at higher angular velocities and air flow rates.

- Particle Elutriation

In an early analysis, Levy et al derived an expression for the terminal velocity of a single particle in a combustor centrifugal force field [2]. Assuming $a_r/g>>1$ the radial gas velocity at which particle entrainment occurs is obtained by relating the inward radial drag force on the particle to its radial acceleration. This leads to

$$u = \sqrt{\frac{4}{3}\left(\frac{\rho_s-\rho_f}{\rho_f}\right)\frac{d_p a_r}{C_D}} \qquad (5)$$

where for spherical particles, the drag coefficient is given as

$$C_D = \frac{24}{Re} + \frac{6}{1+\sqrt{Re}} + 0.4 \quad .$$

An upper bound on the air flow rate beyond which significant particle entrainment occurs can be calculated by evaluating equation (5) at the inner surface of the bed ($r = r_i$). The stability of the particles is illustrated in Figure 13 where radial drag and acceleration are plotted versus radius. To a first approximation the radial drag on a single particle varies as $1/r$. The radial acceleration varies as $1/r^3$ in the freeboard. Consider an experiment where the combustor angular velocity is constant and the air flow rate increases from minimum fluidization conditions. Curves 1-3 describe the condition where the radial acceleration is greater than the drag for all values of radius. There is no tendency for particles to be entrained. Curve 4 describes the condition where the radial acceleration is balanced by the drag force from r_i to r_o and exceeds the drag force for $r<r_i$. Any particle thrown inward radially from the bed would be forced back into the region of the bed, preventing entrainment. Curve 5 illustrates a condition of instability, where the bed can detach from the wall, but where particles are prevented from moving to radii less than r_e. The air flow rate for curve 6 is large enough to carry particles past r_e and out of the combustor.

The analysis illustrated in Figure 13 gives an upper bound on the air flow rate beyond which significant particle entrainment would occur. Phenemena, such as bubbling and particle transport through end wall boundary layers in the freeboard, would tend to cause particle loss from the combustor at gas flow rates which are lower than those given in the figure.

A series of experiments is planned to provide insights into the mechanisms for particle loss from a CFB and to provide criteria for calculating the onset of particle entrainment and for determining particle entrainment rates as a function of CFB operating conditions. To accomplish this, one of the three CFB test sections is being modified to permit controlled experiments of particle elutriation.

A cyclone for particle collection was purchased and design and fabrication of the rotating seal and connecting ducting was initiated. After the system is installed, and checkout and calibration are completed, the experiments on particle loss will be initiated.

- Plans for Next Quarter

During the next quarter the batch experiments will be continued to gather more data on system fluidization. The development of hardware for the elutriation studies will be continued and when completed, experiments on particle elutriation will be initiated. Studies of solids feeding and removal will be continued to gather additional information on the operating characteristics of the feed and removal systems.

TASK 2

- Fluid Mechanics of Confined Vortex Flows

This task involves a study of the fluid mechanics of confined vortex flows without particles. Previous work on these flows indicates that nonuniformities in radial velocity, secondary flow patterns and flow instabilities can occur. The present investigation is intended to develop criteria for the flow regimes in which secondary flow patterns occur and to determine the influence of these phenomena on bed stability, uniformity of fluidization, and particle entrainment. Work has been in progress for several months to develop the capabilities of measuring the flow patterns and velocity profiles in the rotating chamber using hot fiber anemometer probes. Calibration techniques, data reduction procedures and an error analysis of voltage signals were described in Reference 3. During the last quarter, exploratory measurements of the velocity profiles in the rotating chamber were initiated.

The test section is a 0.29 m diameter and 0.127 m high cylinder which rotates about its vertical axis of symmetry. The cylindrical distributor wall is constructed of perforated steel sheet covered with

foam rubber to minimize velocity variations along the grid. The top and bottom end walls, made of plexiglass sheet, rotate with the distributor. The exit opening of the chamber is 0.14 cm in diameter.

Air is delivered to the plenum chamber by a centrifugal blower at a maximum flow rate of 800 scfm. The test section is rotated by a variable speed electric motor at angular velocities up to 200 rpm.

The measurements in the chamber are made by moving the fiber film probe vertically from top to bottom at each of four radial positions: 0.25 r_o, 0.50 r_o, 0.75 r_o and 0.90 r_o (Figure 14). To minimize probe damage, the probe support is equipped with a sensing arm to prevent the probe tip from striking the moving end walls. This permits the probe tip to be moved to within 0.5 cm (0.2 in.) of the end walls.

The probe holder is designed to orient the probe body at a 45° angle with respect to the vertical to minimize wake effects and permit measurements in the upper portion of the chamber. At the 0.75 r_o and 0.90 r_o positions, the measurements are made in the top half of the chamber with the probe body angled up, and the rest of the data are taken with the probe body angled down. In the exit plane the probe is moved radially from the outer exit radius, r_e, to a point approximately 1.3 cm past the centerline. Sample radial and tangential profiles are shown in Figures 15 to 17 for a flow rate of 500 cfm and an angular velocity of 125 rpm. This corresponds to values of radial and tangential Reynolds number of

$$Re_N = \frac{u_o r_o}{\nu} = 1.8 \times 10^4$$

and

$$Re_T = \frac{\omega r_o^2}{\nu} = 1.6 \times 10^4$$

The data show severe nonuniformities in radial velocity developing in the upper portion of the chamber. The acceleration of the flow in this region at $r/r_o = 0.90$, 0.75 and 0.50 is due to the convergence of the streamlines near the exit plane.

More work is needed to determine if the vertical irregularities in tangential velocity at $r/r_o = 0.9$, 0.75 and 0.5 in Figure 17 actually exist in the undisturbed flow or are due to probe disturbances or other types of probe errors. An indication of a wall boundary layer effect is evident at the bottom end wall ($z \approx 0$) for $r/r_o = 0.25$ in both Figures 16 and 17.

The radial variations in axial velocity across the exit plane are shown in Figure 18. Due to system rotation, the axial velocity component decreases in magnitude near the axis of rotation.

- Plans for Next Quarter

During the next quarter, data will be obtained over a wide range of conditions to determine the effect of radial and tangential Reynolds number on wall boundary layer behavior, flow convergence, and viscous core configuration.

APPENDIX

- Cost of Energy for Centrifugal Fluidized Bed Coal Combustion Systems

In another paper [4], Shakespeare et al calculated net cycle efficiencies and energy costs for various coal fired generation system alternatives, including cycles with centrifugal fluidized beds. The CFB system of prime interest utilizes a pressurized CFB coal combustor operating in a combined cycle. Shown in Figure 2, the cycle consists of a compressor supplying air to an adiabatic centrifugal fluidized bed coal combustor. The hot gas passes through a particulate clean-up system before entering a gas turbine which drives the compressor and a generator. The gases leaving the turbine contain sufficient energy to generate steam in a boiler which is fed to a steam turbine driving its generator.

The calculations assume a 10:1 pressure ratio across the gas turbine with compressor and turbine efficiencies of 85 and 87 percent respectively. The gases leave the combustor at 871°C, and auxiliary losses through the combustor and related equipment are estimated to be six percent of the cycle electrical output.

The results indicate that for these conditions, a CFB combined cycle has the same efficiency as a combined cycle using a conventional PFBC (38-40 percent).

In Shakespeare's analysis, energy costs were calculated as a function of plant capacity at base load conditions. The values of the parameters used in the analysis are shown in Table 1 and the results are summarized in Figure 19. Curve 1 is an atmospheric pressure CFB steam cycle and curve 3 is a pressurized CFB combined cycle. Curve 4 is a conventional one "g" AFBC steam cycle and curve 5 is a conventional one "g" PFBC combined cycle. Curve 2 is a pulverized coal power plant with flue gas desulfurization. These results suggest that at base load conditions, the centrifugal fluidized bed combustor operating in a pressurized combined cycle is competitive in energy costs with other power generation cycles using conventional fluidized bed combustors. The centrifugal fluidized bed system operating at atmospheric pressure is more expensive than the others due to a relatively low cycle efficiency.

The rotational nature of the CFB combustor may give it operational advantages such as wider load variation than is possible with a one "g" FBC. Because of the excellent turndown capabilities of the CFB combustor,

Table 1
Base Values of Parameters Used in Analysis

Fixed Charge Rate	18%
Fuel Cost	\$8.04 x 10^{-4}/MJ(85¢/10^6BTU)
Sulfur Content of Coal	3.9%
Sorbent Cost	\$10/ton
Operation & Maintenance	1.5 mills/kWh
Construction Period	5 years
Escalation Rate	6.5%
Interest Rate	10.0%

this system might prove particularly attractive operating at peak load conditions. To study the economics of the CFB coal combustion system operating at peak load conditions, an analysis was performed which compares two CFB coal combustion systems with a number of other coal based power generation alternatives [5].* The results are shown in Figure 20, expressed as cost of electricity versus capacity factor for a 600 MWe power plant. All of the costs are expressed in 1974 collars.

The analysis assumes that naturally occurring petroleum and pipeline gas are unavailable, requiring that electricity be generated either by direct combustion of coal or by combustion of synthetic fuels from coal. It is also assumed that coal gasification systems will be able to operate only at base load conditions, making a low or medium BTU gas fired combined cycle system unavailable for peak load conditions. Gas turbine grade synthetic liquids are estimated to cost \$5.00/10^6BTU.

Curve 1 (Figure 20) is a simple gas turbine burning a synthetic liquid fuel, and curve 2 is a simple gas turbine operating with an adiabatic pressurized CFB coal combustor. The pressurized CFB combustor operating in a combined cycle is given by curve 6. The other alternatives are assumed to be available only for base load operation, but are included here for comparison. These include the pulverized coal combustor with flue gas desulfurization (curve 3), combined cycles with synthetic gaseous fuels at \$2.50/10^6BTU and \$1.50/10^6BTU (curves 4 and 7) and a simple gas turbine with a gaseous fuel at \$2.50/10^6BTU. Curves 3, 5 and 7 are taken from the ECAS study [6].

The results show that of all the alternatives, the CFB coal combustor operating in a combined cycle is the cheapest in the peaking range. As shown in the previous figure, this system is also competitive with the alternatives at base load conditions.

*Performed by Dr. D. Kroger, Visiting Professor of Mechanical Engineering and Mechanics.

SUMMARY AND CONCLUSIONS

Separate experiments were performed with materials of two different densities and with two different types of particle size distributions to test the validity of the theoretical models. The results show that particle density has a strong influence on minimum fluidization and fluidized bed pressure drop. The particle size distribution has an influence on the packed bed pressure drop and transition to a fluidized state. The effects of both parameters are predicted well by the theory.

Preliminary experimental results from the fluid mechanics study have now been obtained, and additional detailed measurements will be made to determine the influence of speed of rotation and gas flow rate on the shapes of the velocity profiles.

An analysis of the energy costs for a CFB coal combustor operating in a combined cycle has been performed. When compared to energy costs for other fossil fired power generation systems, the results indicate that the CFB system has excellent potential for peak power generation applications.

REFERENCES

1. "Centrifugal Fluidized Combustion of Coal - Annual Report," FE-2516-4, October 1977.

2. Levy et al, "Parametric Analysis of a Centrifugal Fluidized Bed Coal Combustor," ASME paper 76HT-68.

3. "Centrifugal Fluidized Combustion of Coal - Quarterly Report," FE-2516-6, April 1978.

4. W. Shakespeare et al, "Analysis of Power Cycles with Centrifugal Fluidized Bed Coal Combustion," Proceedings 1977 Intersociety Energy Conversion Engineering Conference, Washington, D.C.

5. D. Kroger, unpublished analysis, Lehigh University, 1978.

6. Comparative Evaluation of Phase I Results from the Energy Conversion Alternatives Study (ECAS), Energy Research and Development Administration and National Science Foundation, NASA TMX-71855, February 1976.

NOMENCLATURE

a_r = radial acceleration

d_p = particle diameter

$Ga = (\rho_s/\rho_f - 1)\omega_o^2 r_o d_p^3/\nu^2$

P = pressure

$Re = u_o d_p/\nu$

r_e = exit radius of chamber

r_i = inner radius of bed

r_o = outer radius of bed

u_o = radial velocity at r_o

V_t = tangential velocity

ε = void fraction

ϕ = sphericity

ρ_f = gas density

ρ_s = solid density

μ = absolute viscosity

ν = kinematic viscosity

ω_o = angular velocity of bed

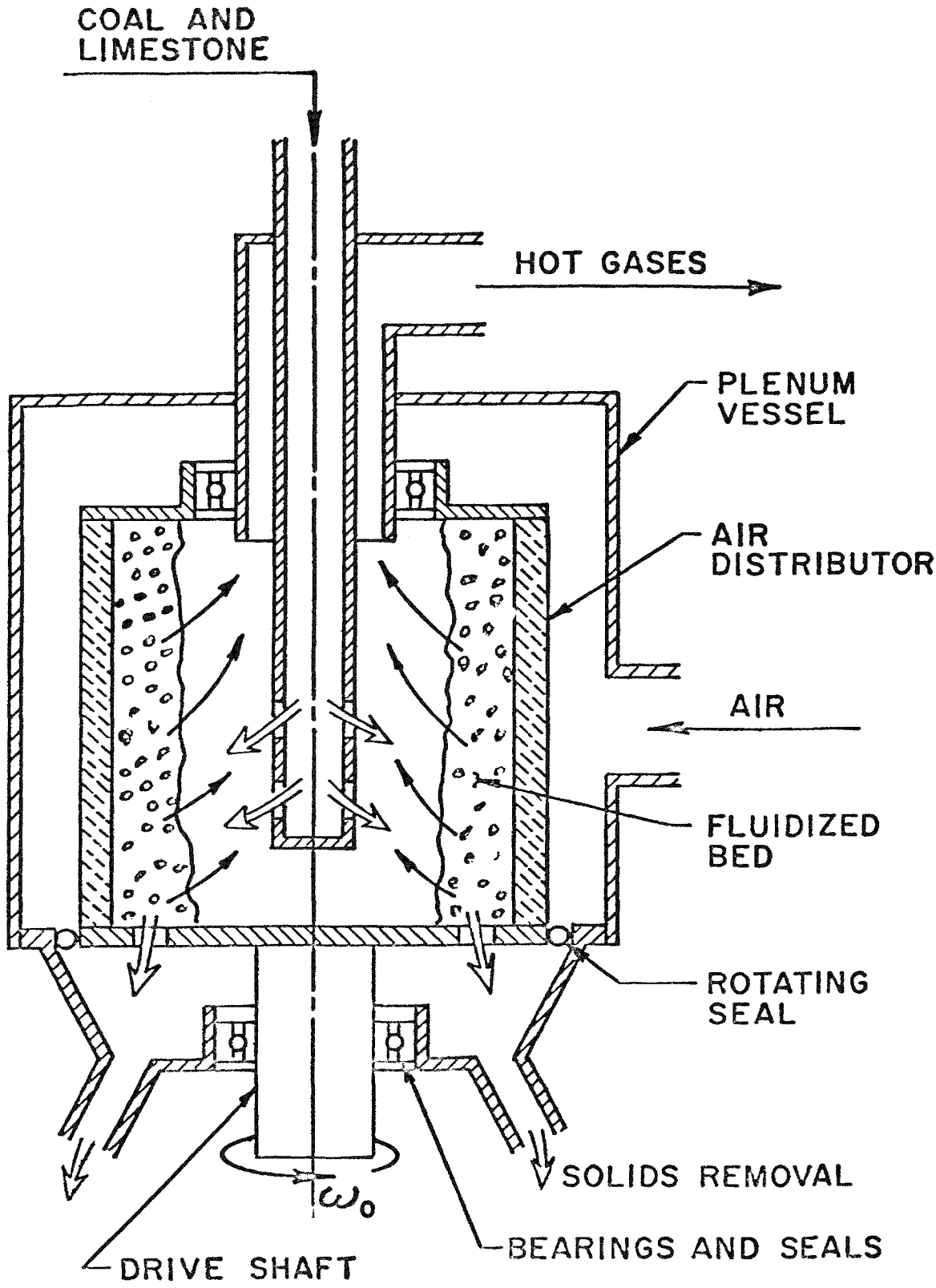

Fig. 1 Conceptual Drawing of Centrifugal Fluidized Bed Combustor

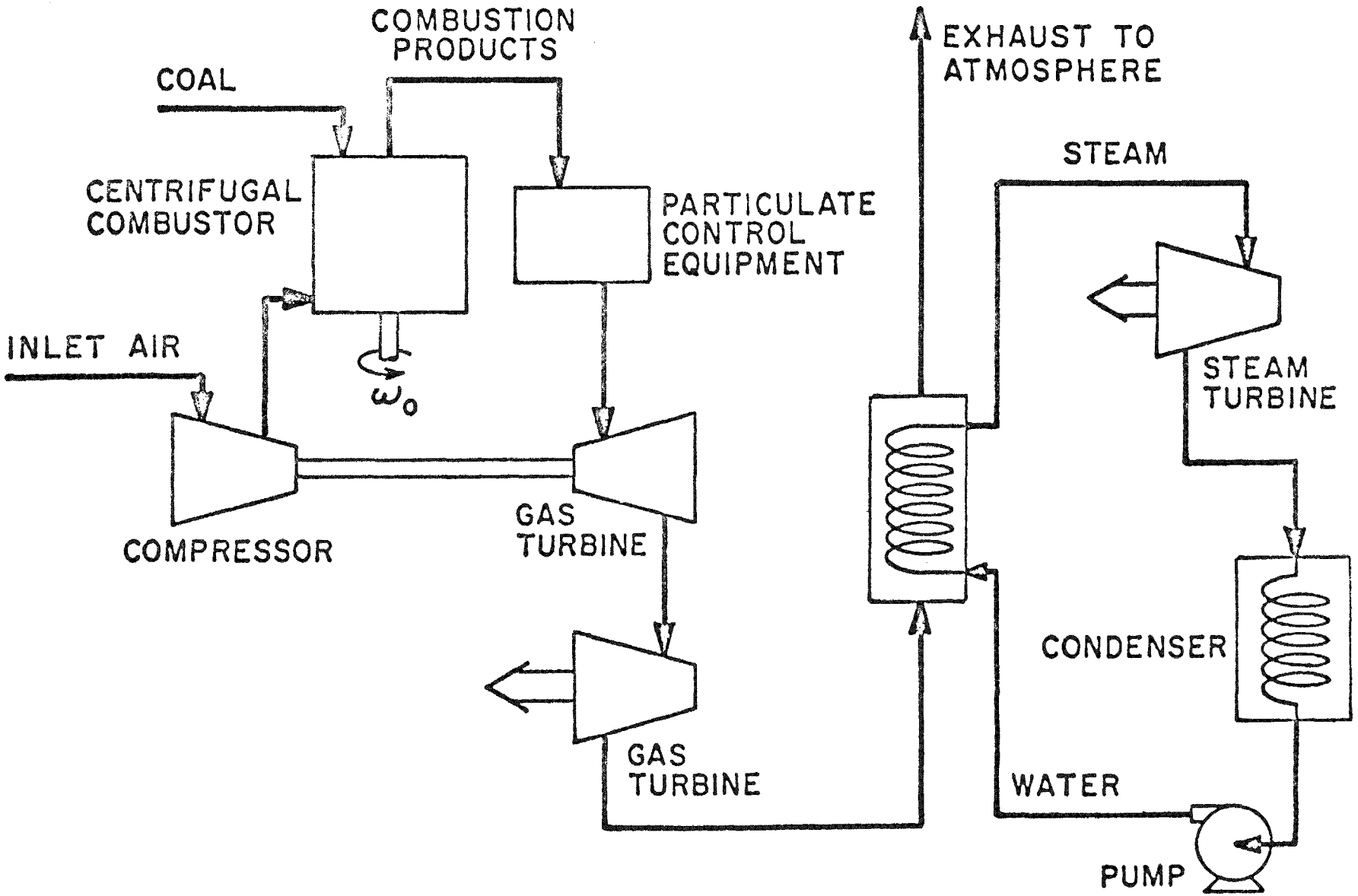

Fig. 2 Adiabatic Combined Cycle Power Plant

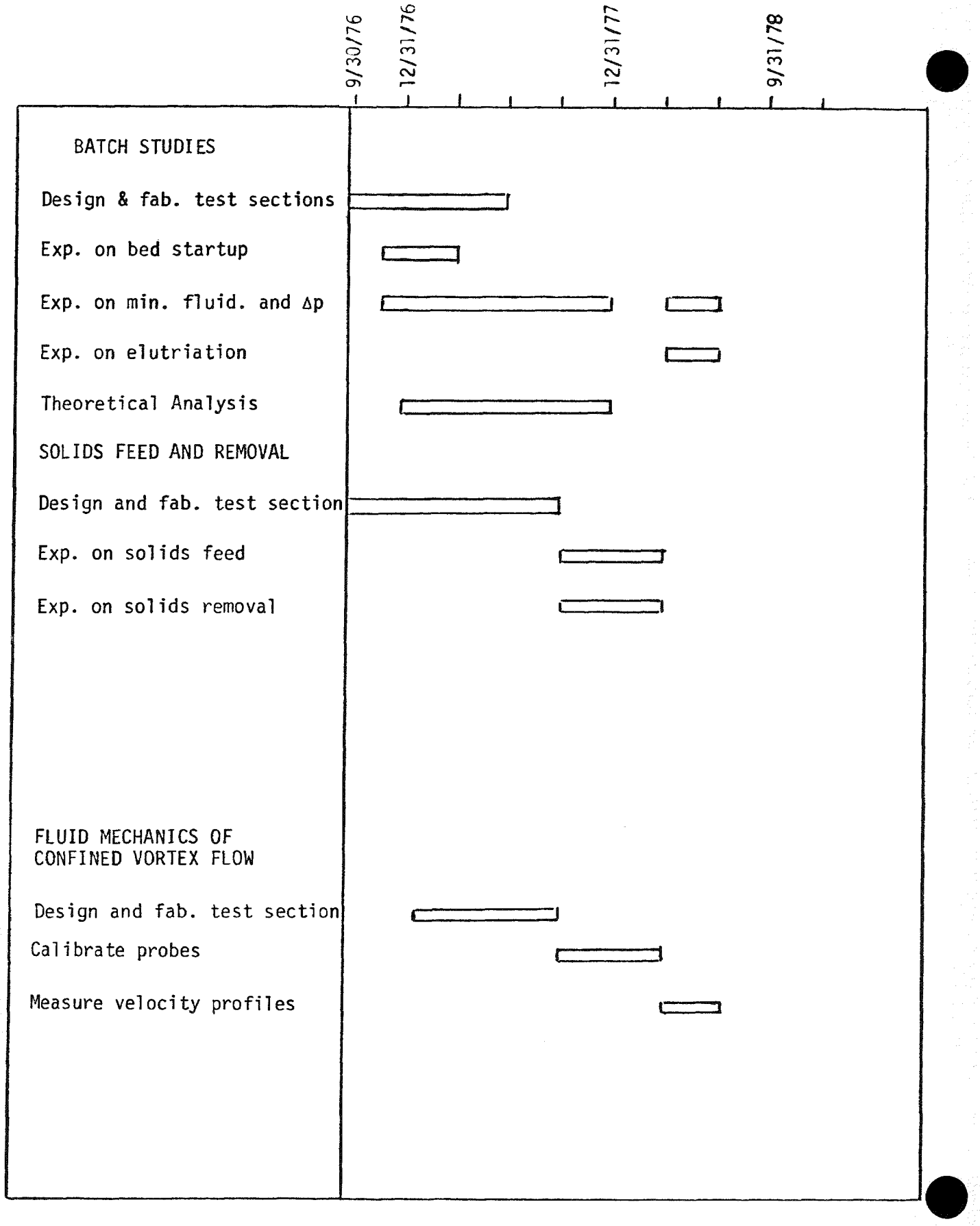

Fig. 3 Project Schedule

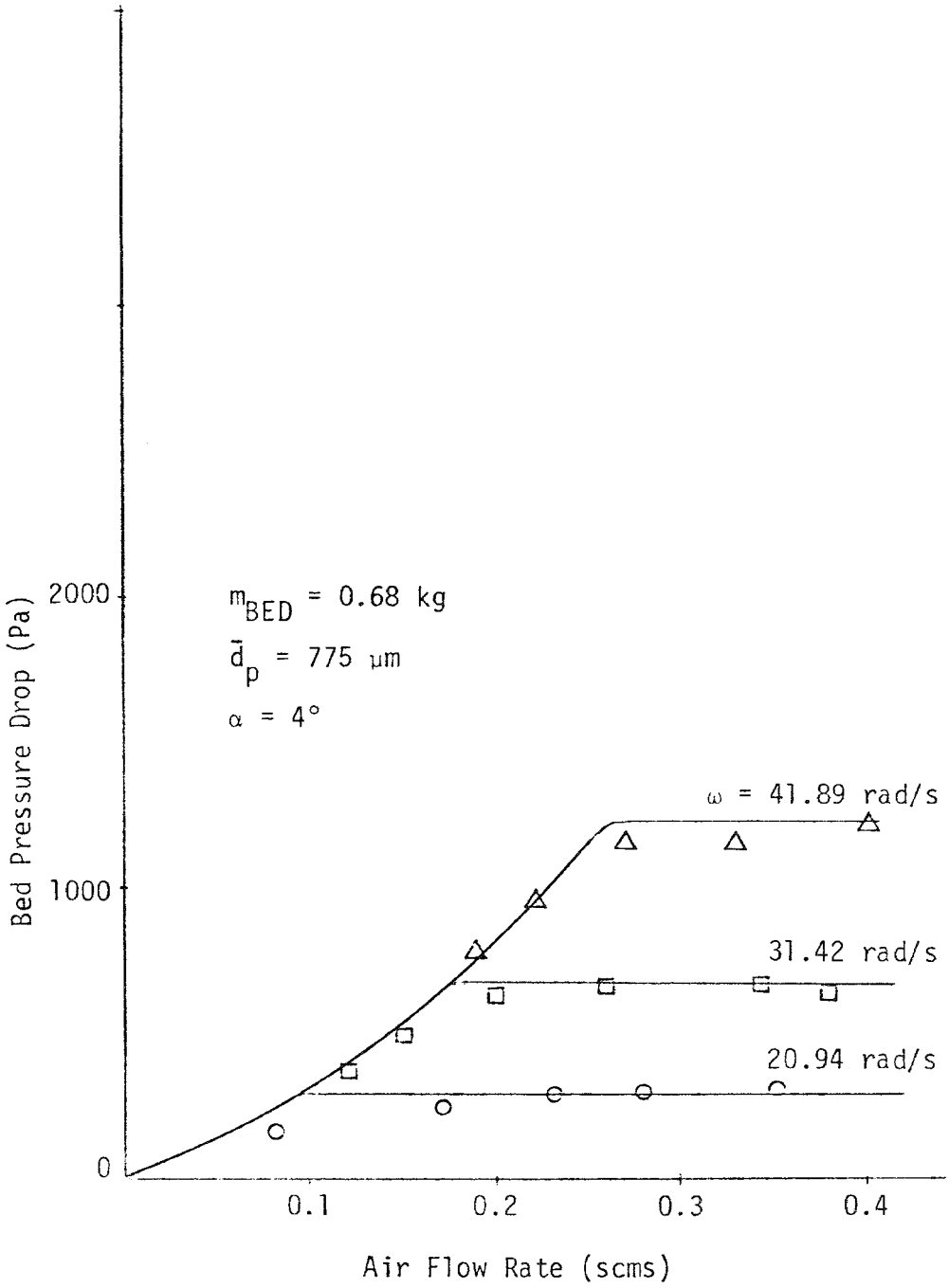

Fig. 4 Effect of speed of rotation on fluidization. Styrene bed with narrow size distribution.

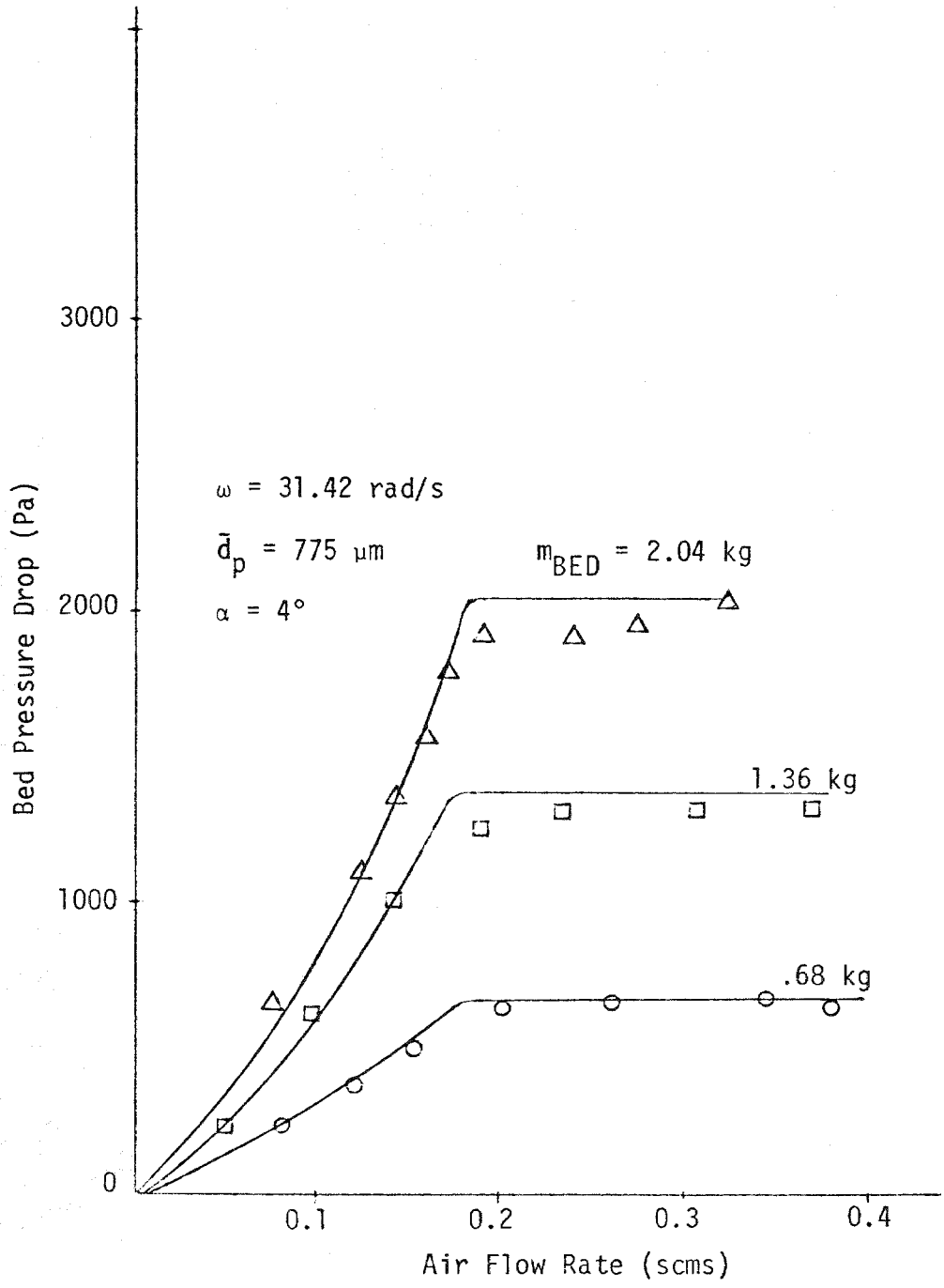

Fig. 5 Effect of bed mass on fluidization for a styrene bed with narrow size distribution

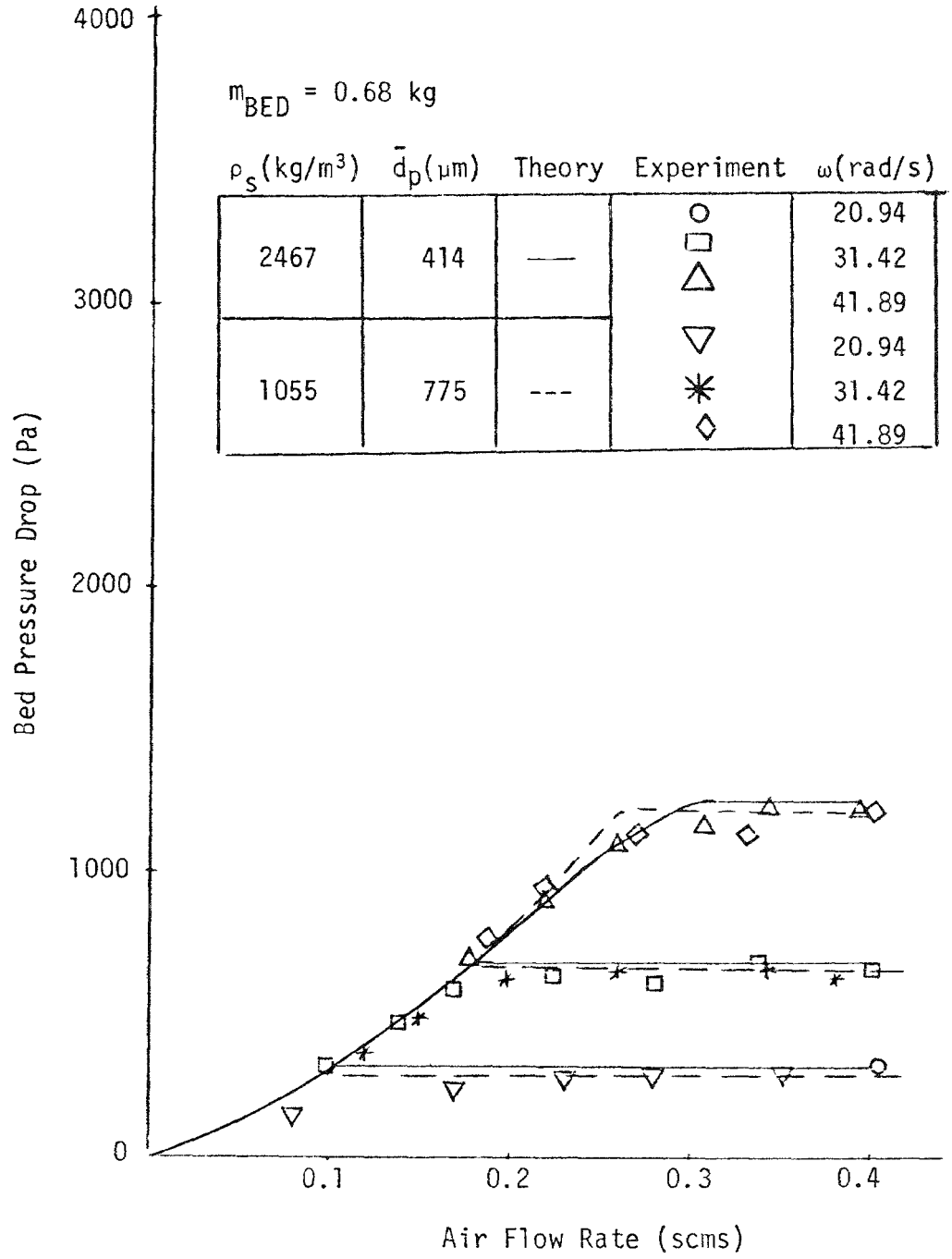

Fig. 6 Effect of particle density on fluidization

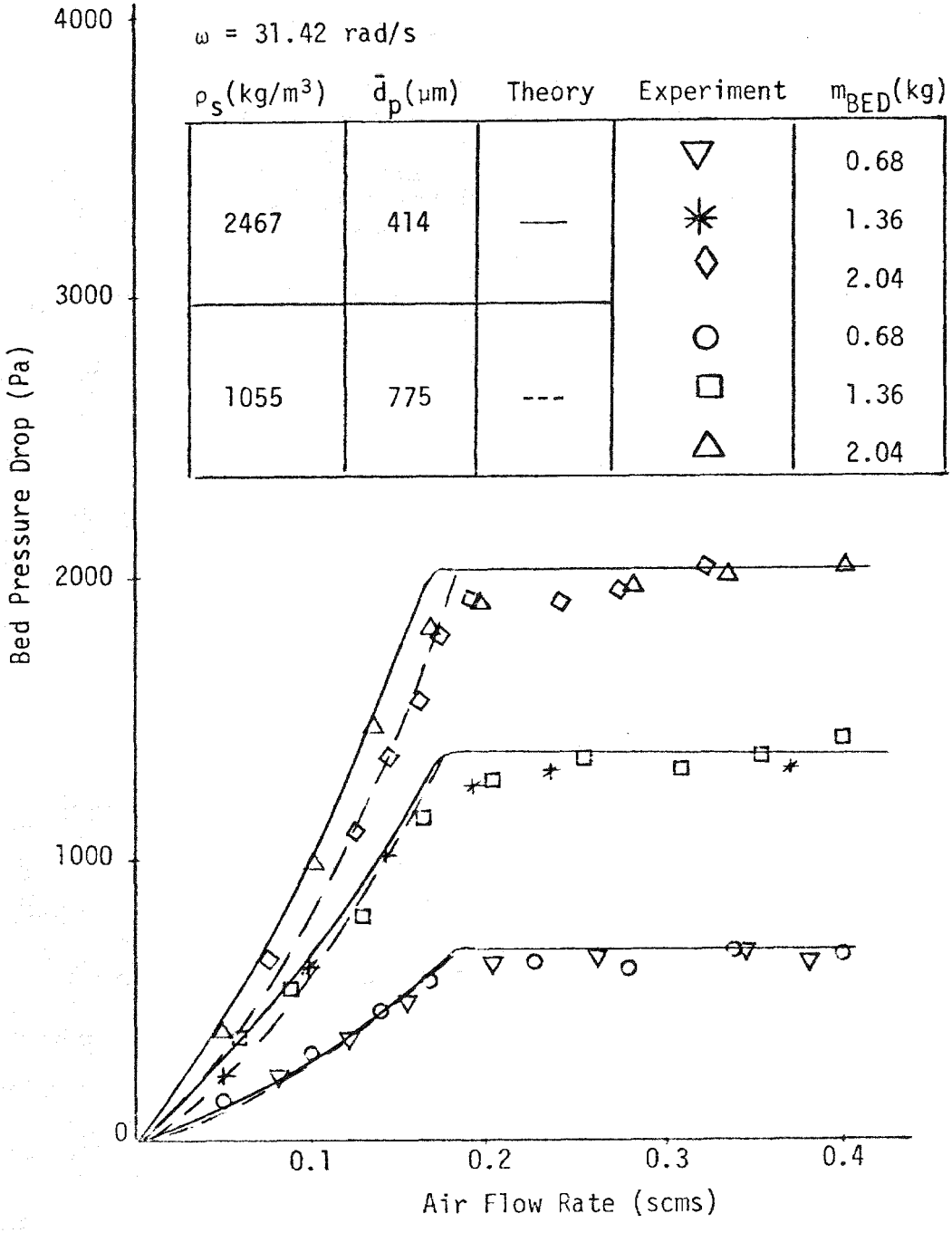

Fig. 7 Effect of particle density on fluidization

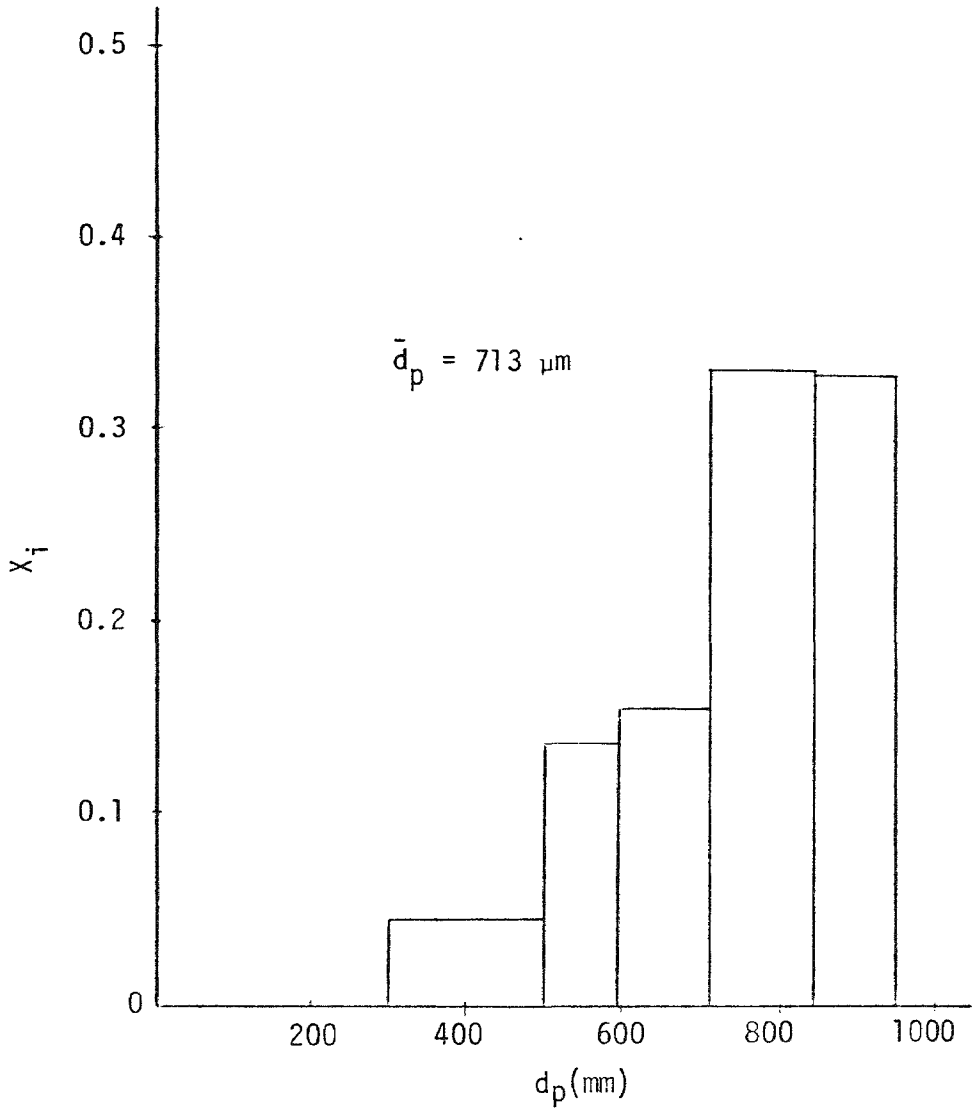

Fig. 8 Size distribution of bed. Styrene beads.

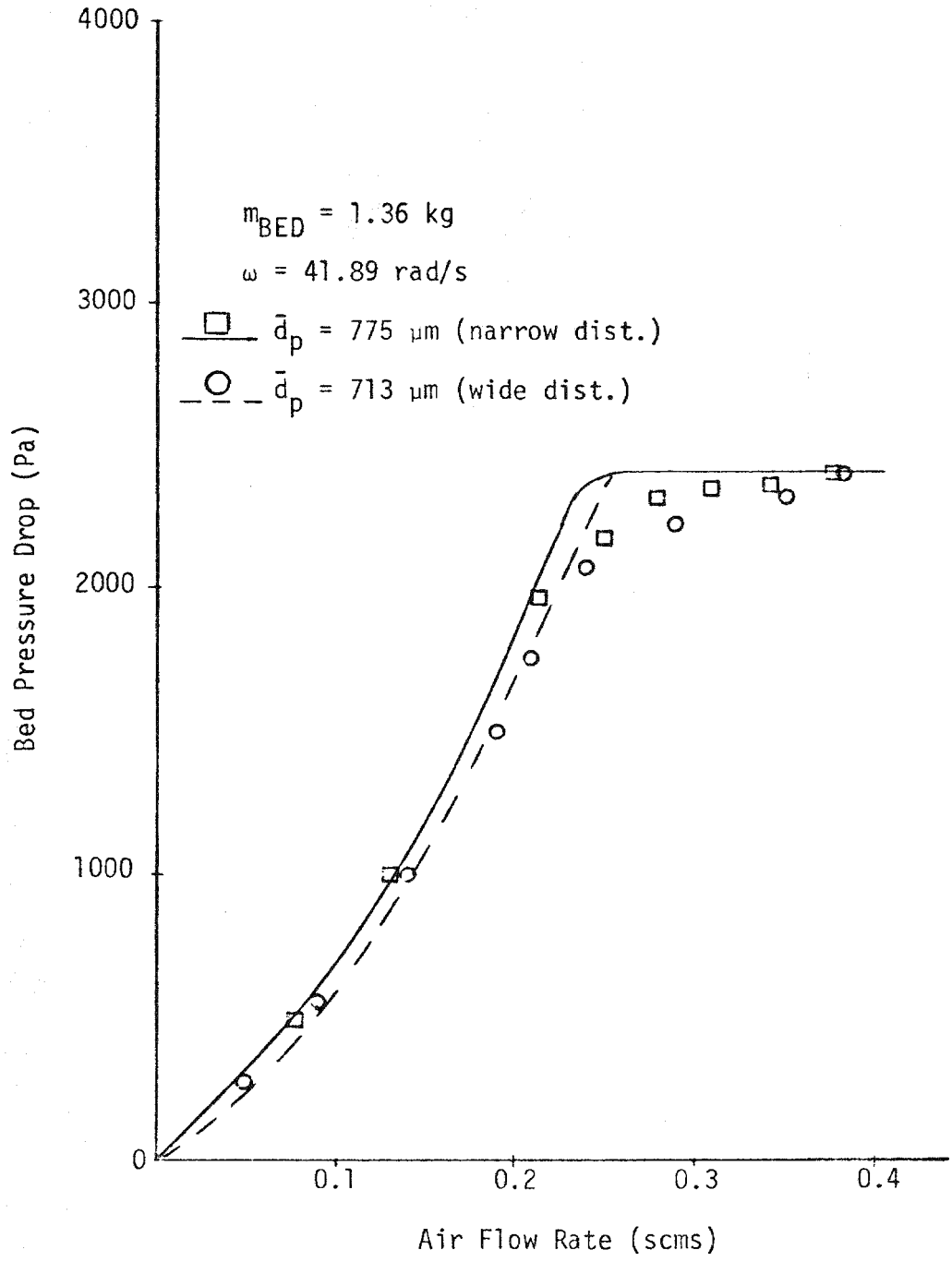

Fig. 9 Effect of size distribution on fluidization for a styrene bed

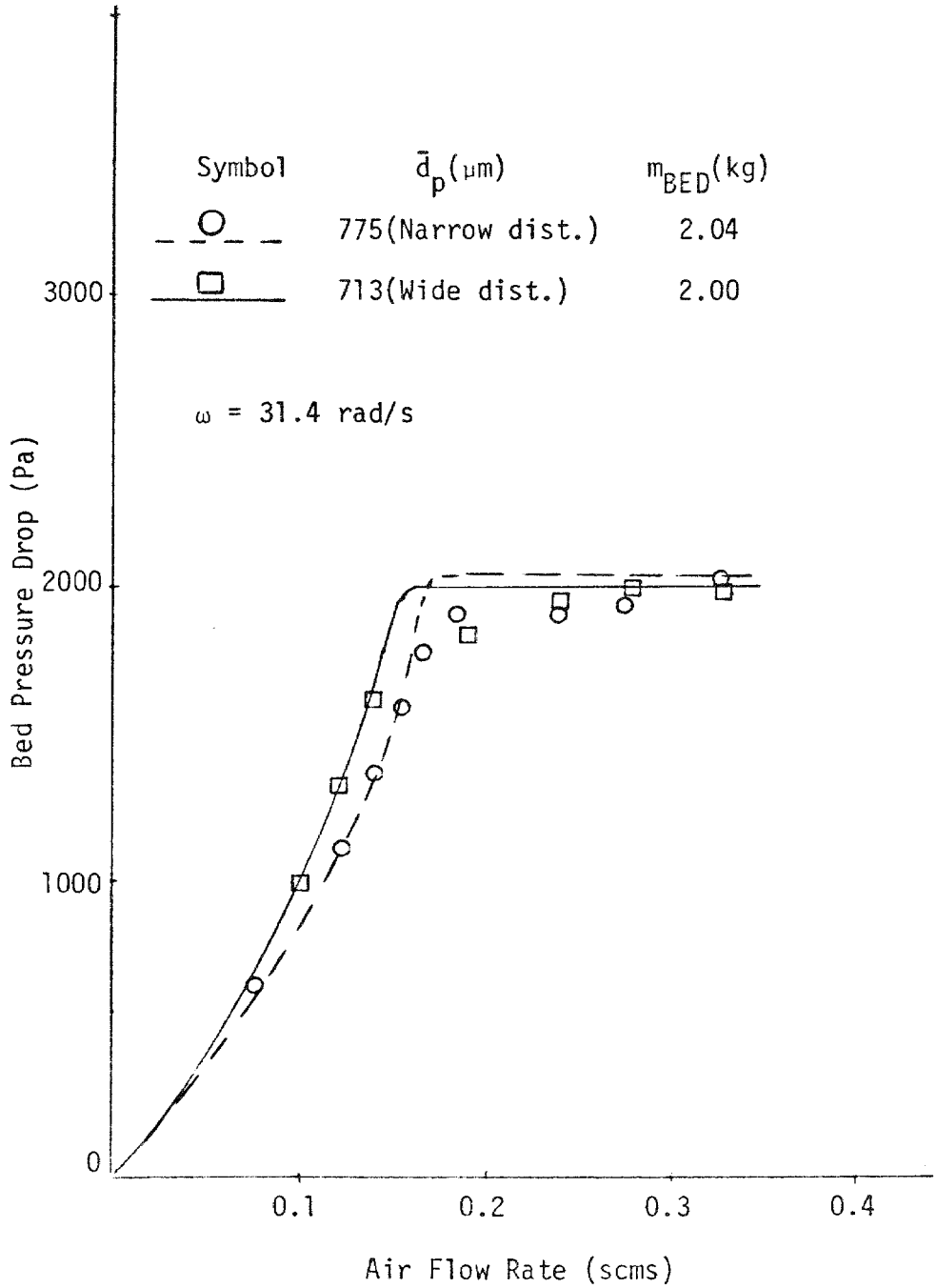

Fig. 10 Effect of size distribution on fludization for a styrene bed

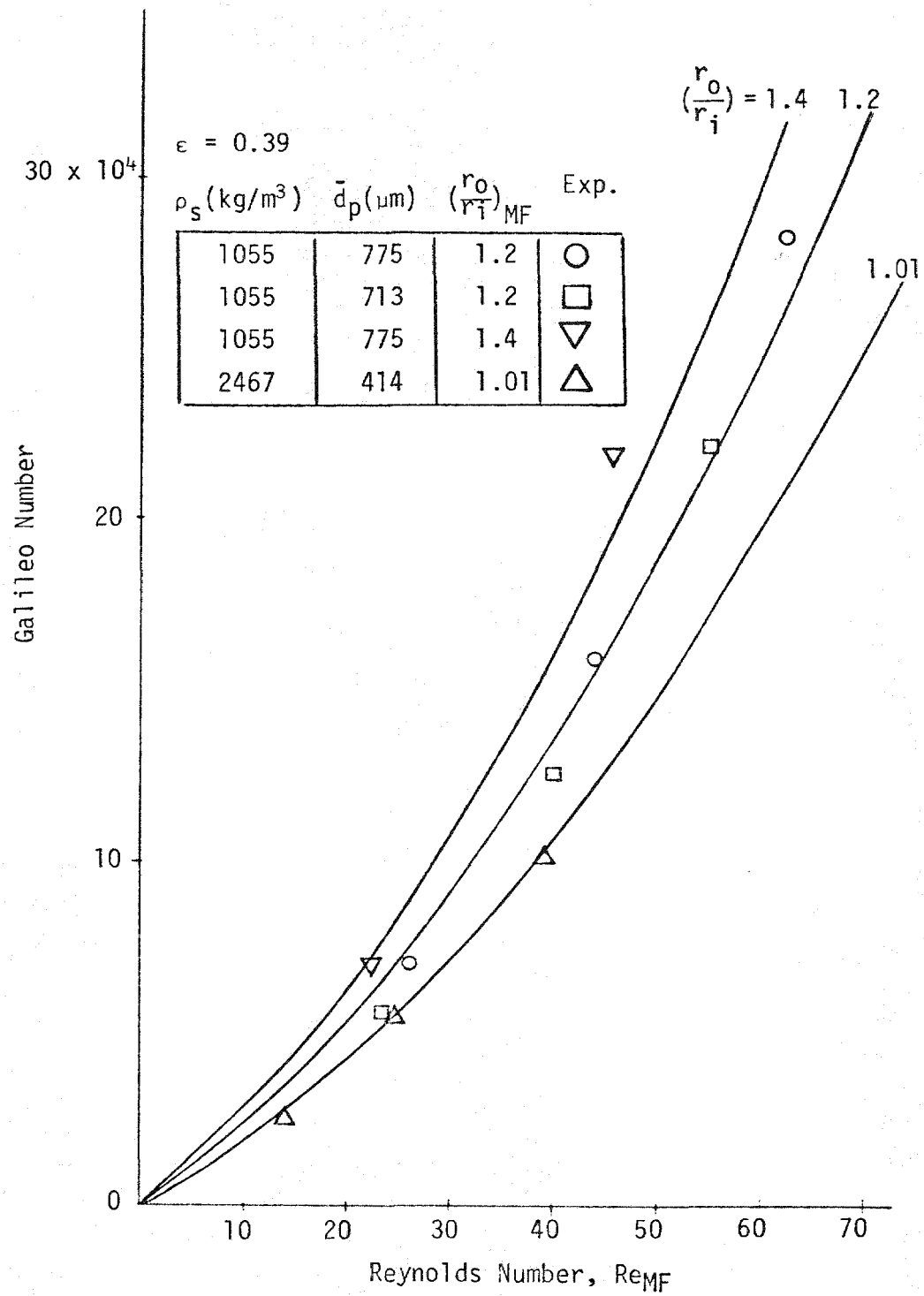

Fig. 11 Comparison of theoretical and experimental results at minimum fluidization

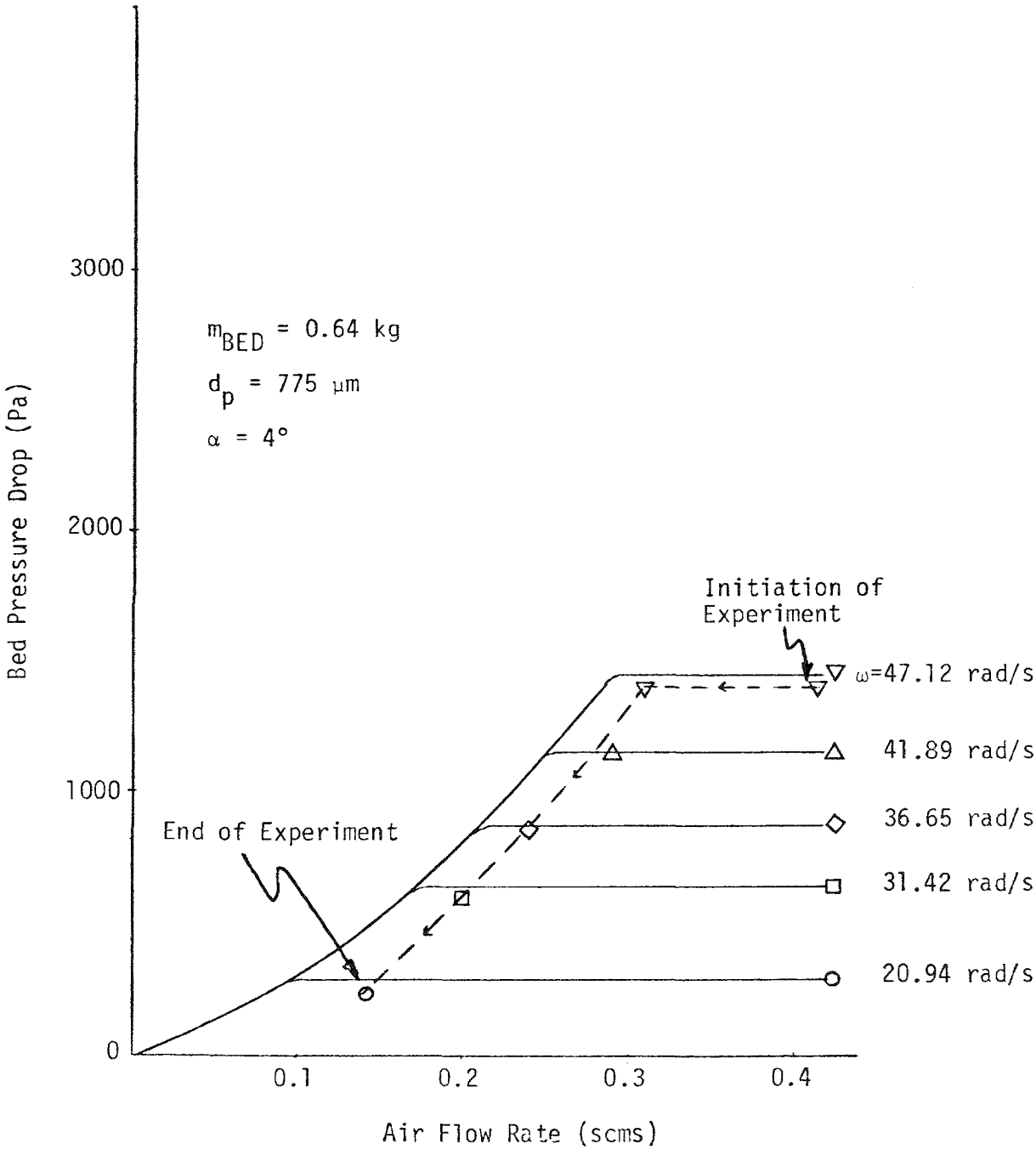

Fig. 12 Illustration of bed turndown. Simultaneous variation of speed of rotation and air flow rate

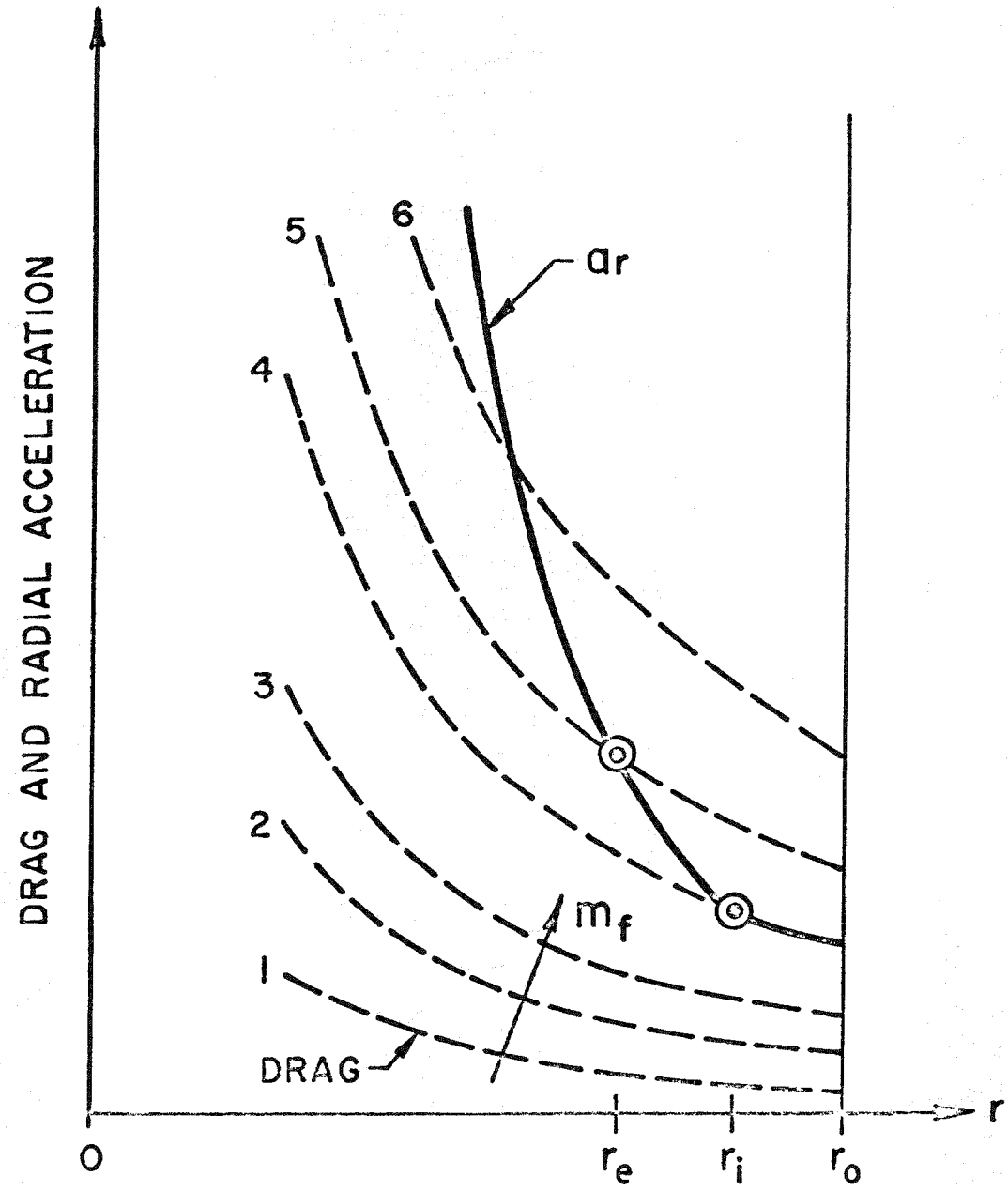

Fig. 13 Illustration of bed stability in CFB combustor

Test Section

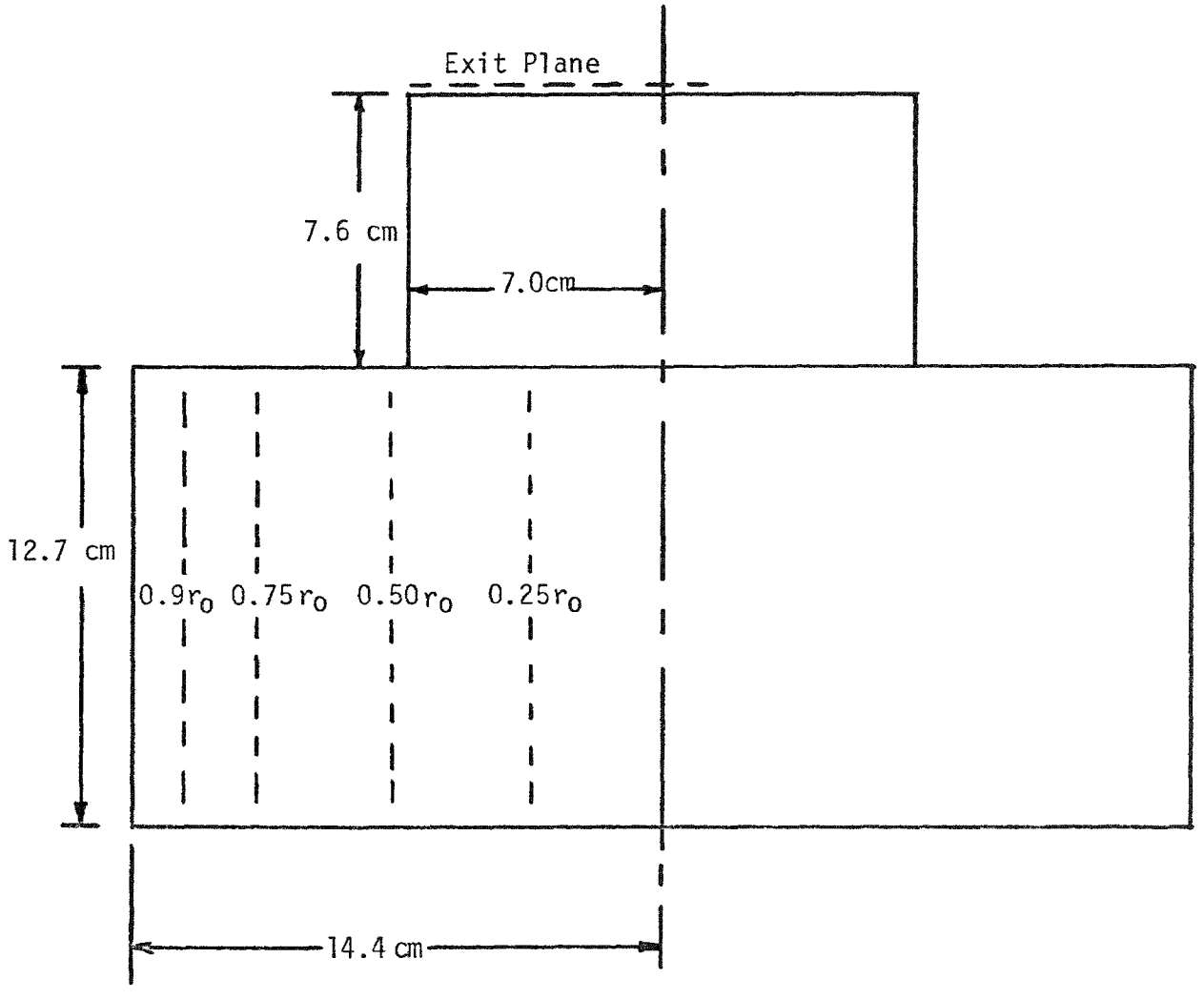

Fig. 14 Sketch of test section

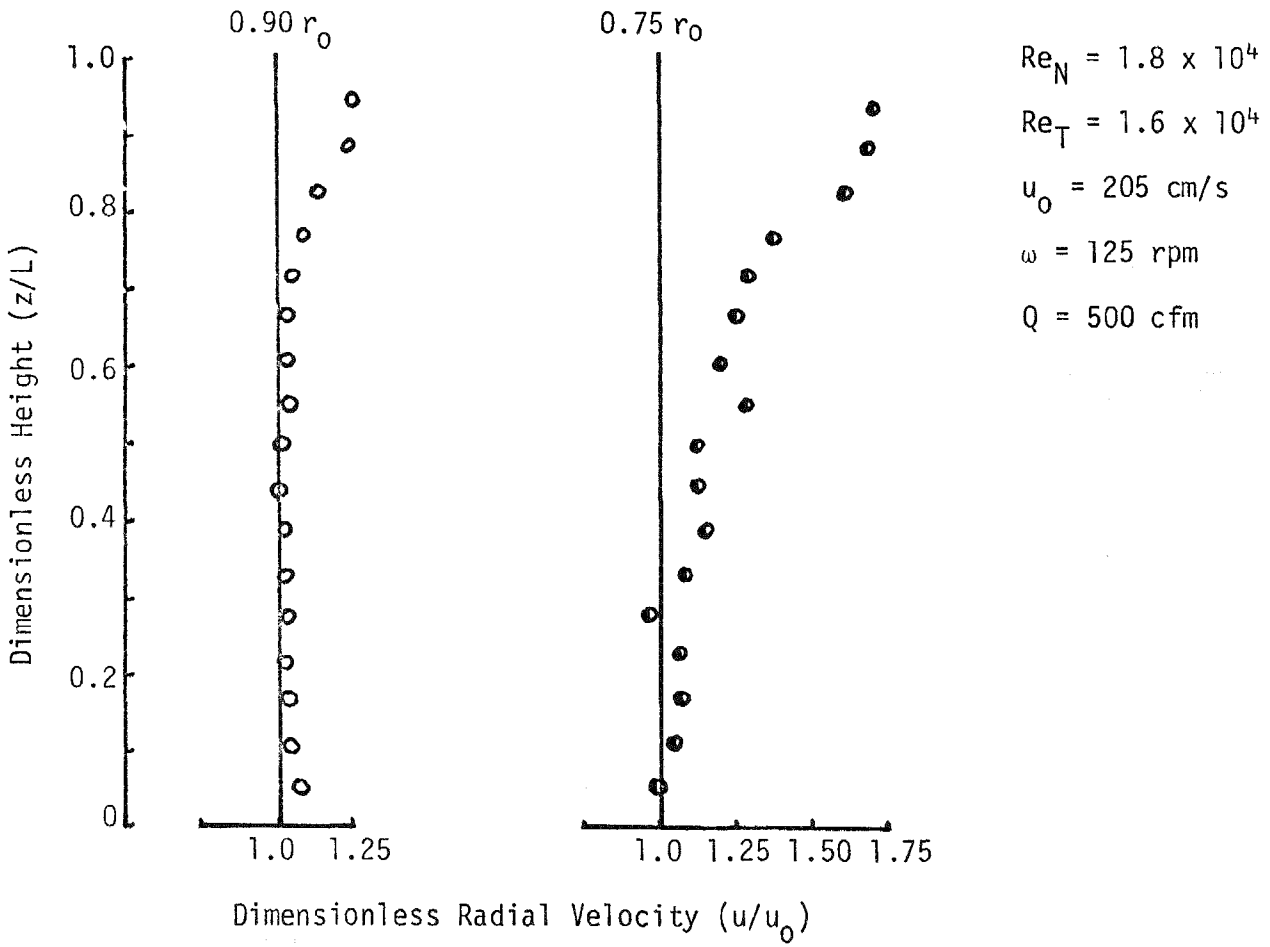

Fig. 15 Radial velocity profiles

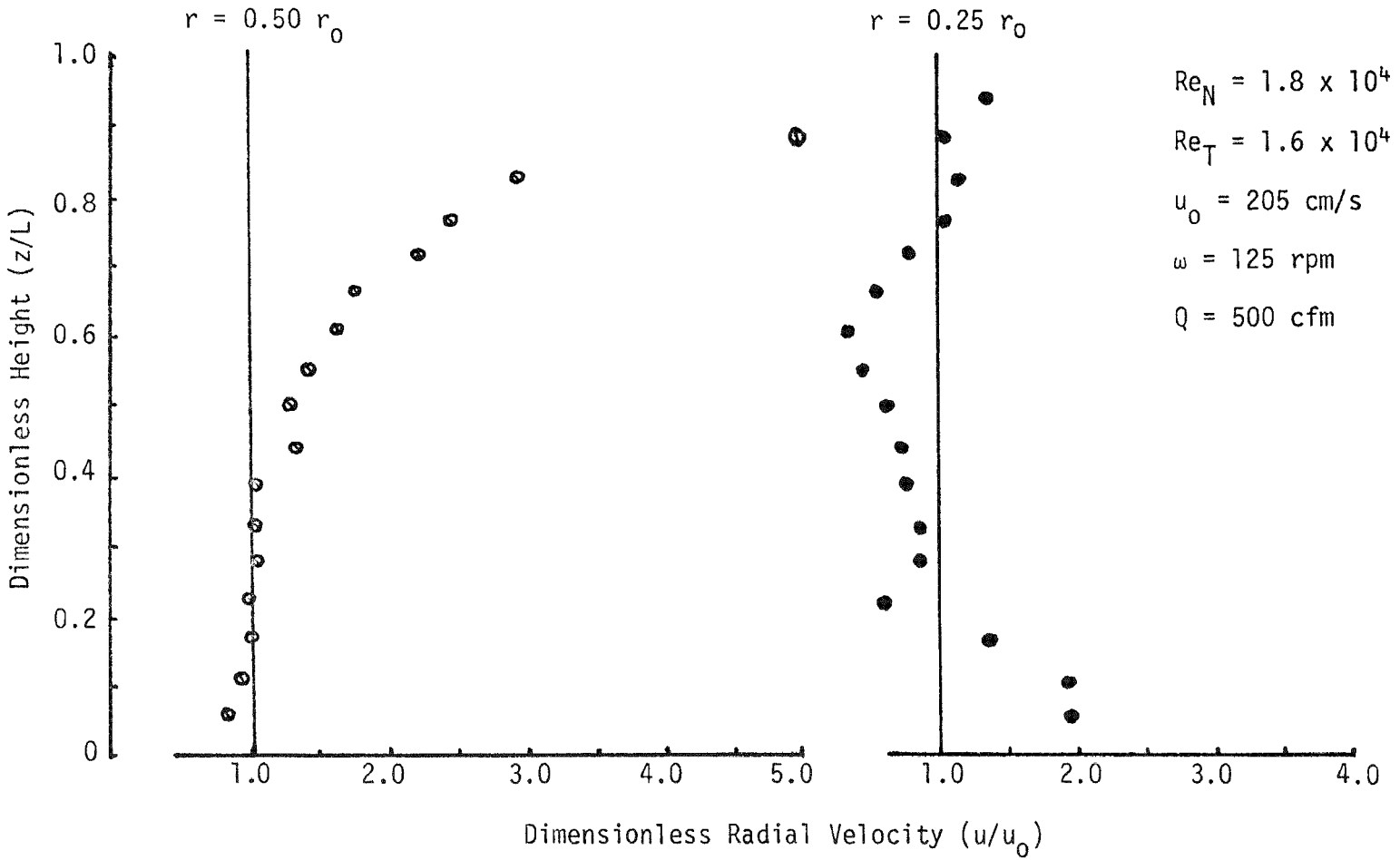

Fig. 16 Radial velocity profiles

V_o = 190 cm/s $\quad Re_N = 1.8 \times 10^4$

Q = 500 cfm $\quad Re_T = 1.6 \times 10^4$

ω = 125 rpm

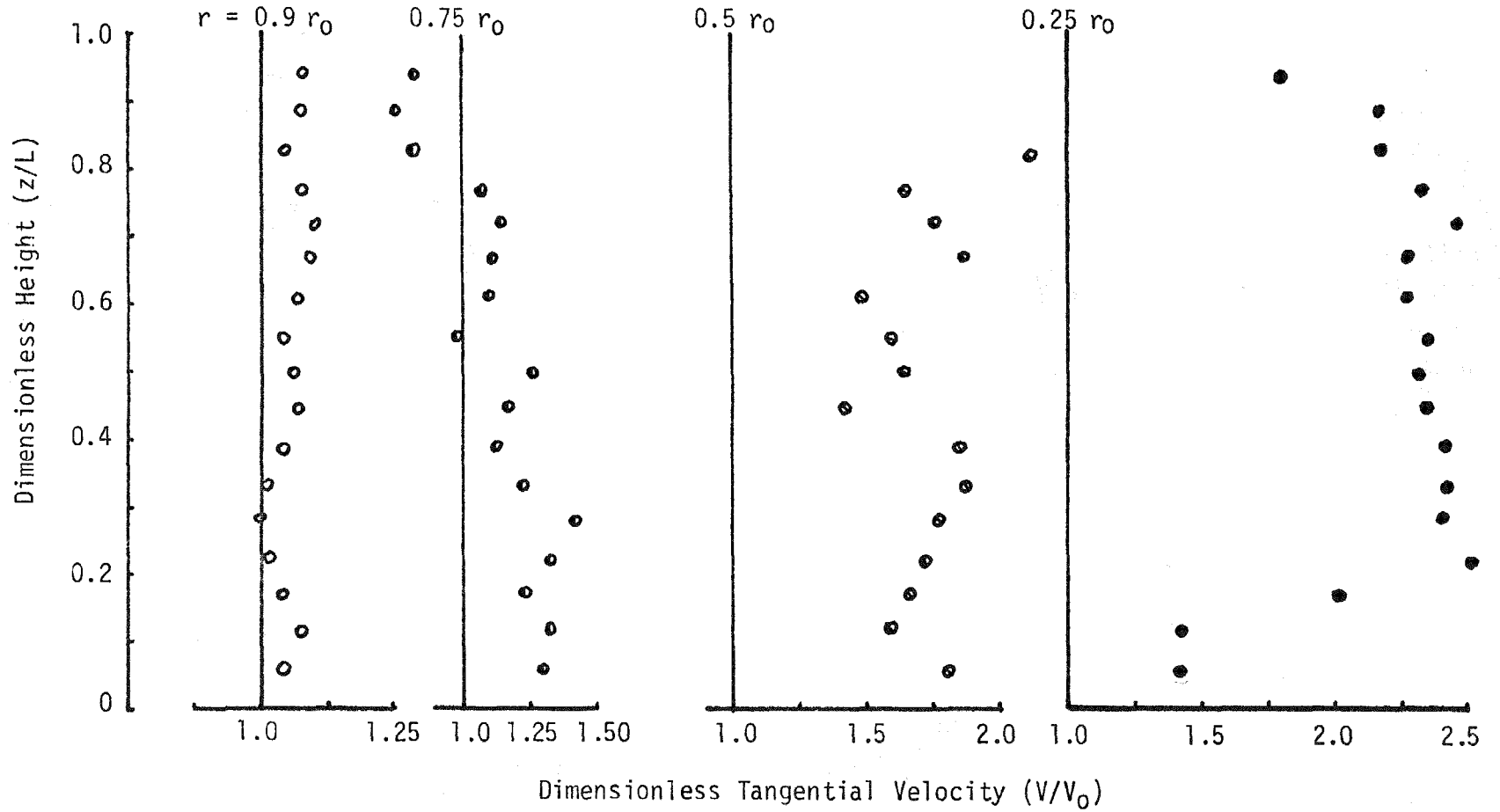

Fig. 17 Tangential velocity profile

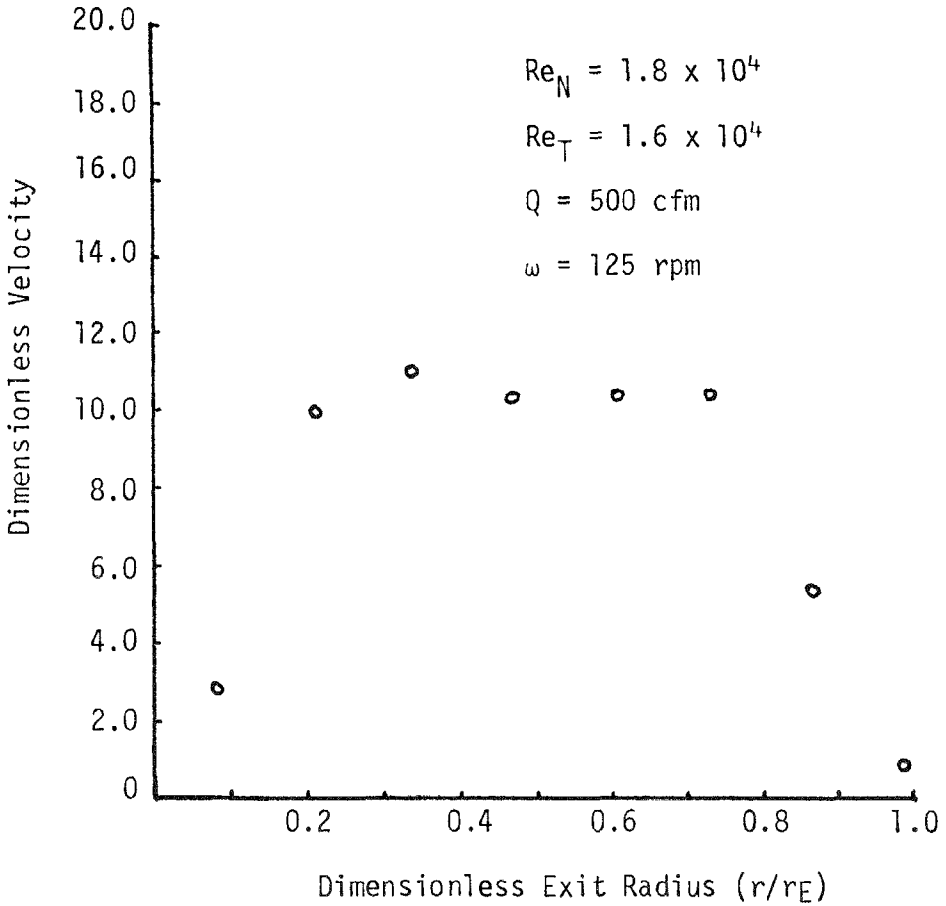

Fig. 18 Exit axial velocity

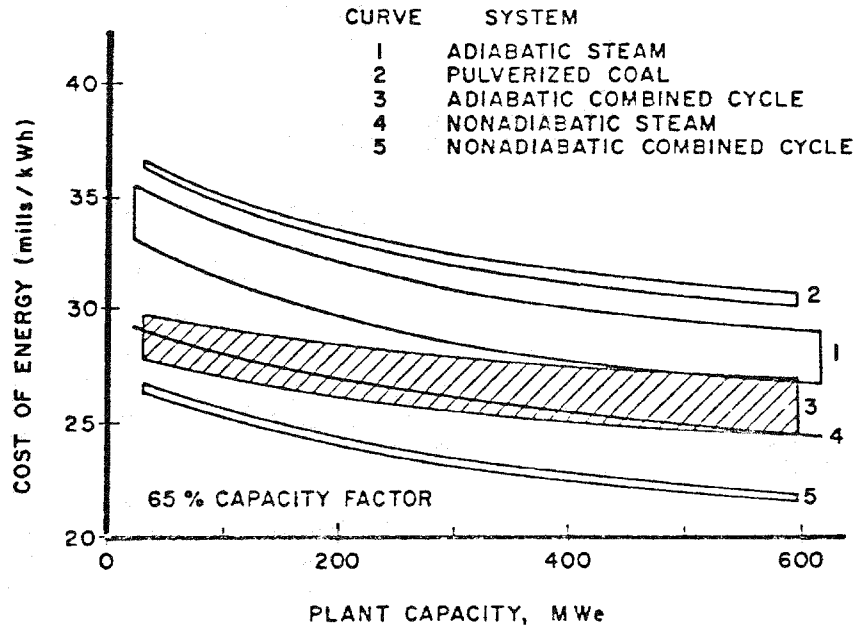

Fig. 19 Cost of electricity at base load operation [curves 1, 3, 4, 5 are FBC systems. Curve 3 is CFB combined cycle.]

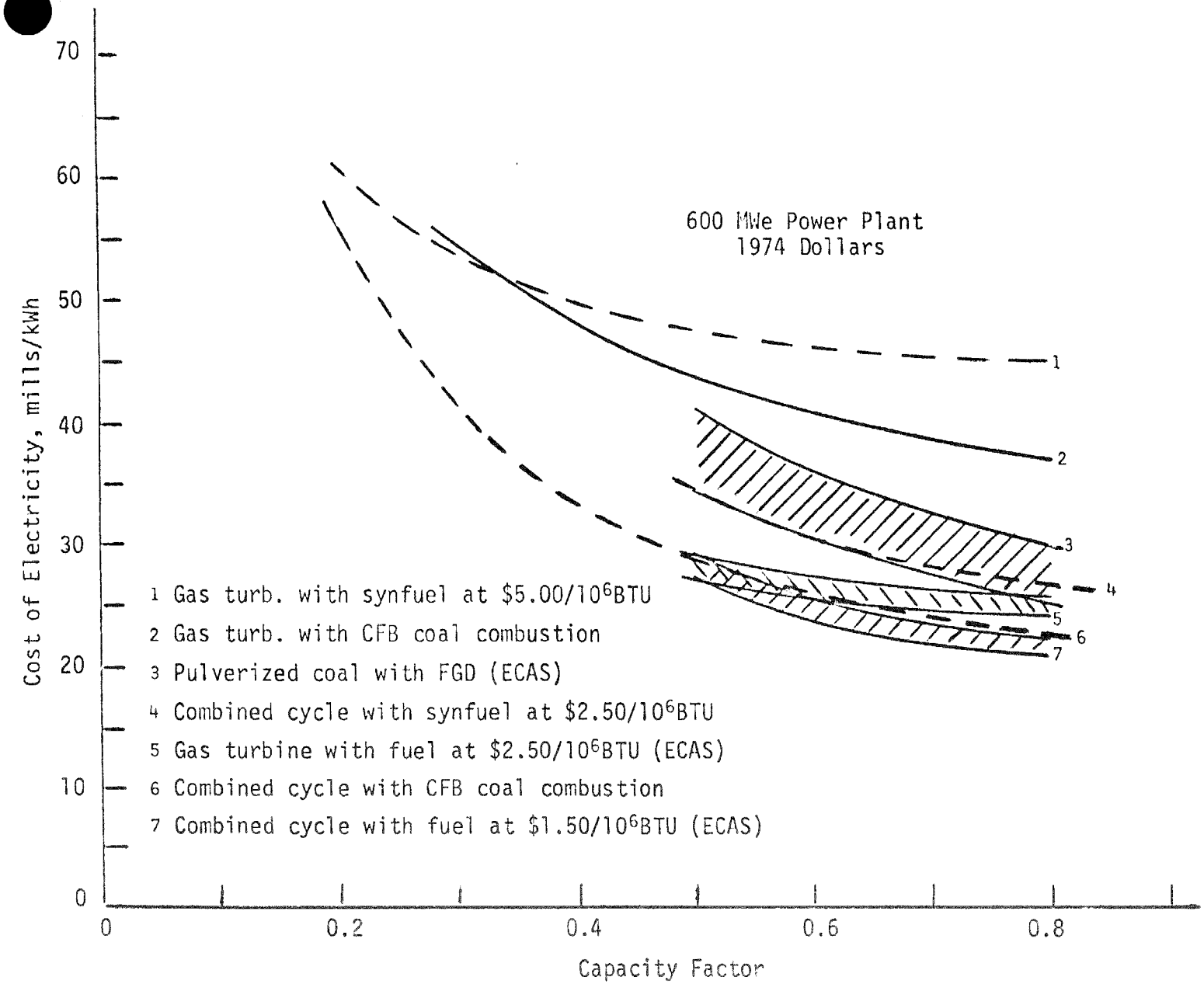

Fig. 20 Cost of Electricity - Advanced Technology Power Plants